

This item is likely protected under Title 17 of the U.S. Copyright Law. Unless on a Creative Commons license, for uses protected by Copyright Law, contact the copyright holder or the author.

Access to this work was provided by the University of Maryland, Baltimore County (UMBC) ScholarWorks@UMBC digital repository on the Maryland Shared Open Access (MD-SOAR) platform.

Please provide feedback

Please support the ScholarWorks@UMBC repository by emailing scholarworks-group@umbc.edu and telling us what having access to this work means to you and why it's important to you. Thank you.

Detecting ship-produced NO₂ plumes and shipping routes in TROPOMI data with a deep learning model

Tianle Yuan^{1,2}, Fei Liu^{2,3}, Lok N. Lamsal^{1,2}, Hua Song^{2,4}

¹GESTAR-II, University of Maryland, Baltimore County, MD, USA

²Climate and Radiation Laboratory, NASA Goddard Space Flight Center, Greenbelt, MD, USA

³GESTAR-II, Morgan State University, MD, USA

⁴SSAI, Lanham, MD, USA

Key points

- We train a deep learning model to detect NO₂ plumes with good performance.
- The detect NO₂ plumes clearly show shipping patterns in the aggregation.
- Our method is useful for emission inventory and emission compliance studies.

Abstract

Ship emissions are important contributor to air pollution and the climate through interacting with clouds. They are the dominant anthropogenic source over the oceans. However, their magnitudes still have large uncertainty. Here we develop a deep learning model to detect ship-emitted NO₂ plumes at the pixel level in TROPOMI tropospheric NO₂ data. The trained model performs well and, when applied to a year of data, it finds major shipping routes, but misses several other routes. We show that high cloudiness in these shipping routes is the culprit because clouds block signals from reach the sensor. Indeed, detected shipping routes in this study complements shipping routes detected using ship-tracks that is only available in cloudy regions. Our method can find application in several areas such as improving ship emission estimates and compliance verifications. Our method will benefit from improved tropospheric NO₂ retrievals since their quality is critical for plume detection.

Plain Language Summary

We train and apply a state-of-the-art deep learning model to detect NO₂ plumes emitted by large ships. The NO₂ concentration is from a new satellite sensor called TROPOMI. Its increased spatial resolution and better retrievals make it possible to detect such ship emitted NO₂ plumes. By applying the model, we can detect individual plumes with excellent fidelity. The aggregated plumes over the global show major shipping routes, but miss other routes. The missing routes are due to high cloudiness in these regions because clouds can block the signals from reaching the satellite sensors. Our method can be potentially useful for monitoring ship emissions of NO_x and verifying compliance of emission standards.

1. Introduction

Ship emissions are significant contributors to air pollution, particularly in coastal areas, and are of great climatic significance by exerting an important influence on marine boundary layer and convective clouds (Capaldo et al., 1999; Yuan et al., 2011). The impact of ship emissions on clouds can be clearly appreciated by the observations of ship-tracks that are often embedded

within marine stratocumulus clouds and show up as long linear and bright, compared to background clouds, features (Conover, 1966; Coakley et al., 1987). Ship emissions are estimated to contribute ~15% of global NO_x emissions and 5–8% of global SO_x emissions (Capaldo et al., 1999; Corbett and Koehler, 2003) and is the dominant anthropogenic source over the ocean. However, there are large uncertainties associated with ship emissions because of uncertainties in locations of activity and in activity levels (Corbett et al., 2010). A robust measurement-based approach to identify the ship emission will complement current emission inventory estimates. Measurement-based approaches can also help to verify the compliance of ship-emission control policies over the open ocean (International Maritime Organization, 2020; Yuan et al., 2022).

Satellite observations of tropospheric NO₂ columns have been widely used to monitor anthropogenic emissions (e.g., Richter et al., 2005; Beirle et al., 2011; Liu et al., 2020; Miyazaki et al., 2017). Several studies have used NO₂ plumes from sources to infer the magnitude and the location of NO_x emissions from individual power plants ((Beirle et al., 2019), gas compressor stations (van der A et al., 2020)), other industrial facilities (Beirle et al., 2020), and cities (e.g., Liu et al., 2016; Goldberg et al., 2019; Laughner and Cohen, 2019; Lorente et al., 2019). Satellite-based NO₂ data have also been used to constrain ship NO_x emissions used in models (Vinken et al., 2014). The detection of plumes from ships is more challenging due to lower signal-to-noise ratio and size of plumes. With improved ground resolution and better signal to noise ratio, TROPOMI observations allow for an improved detection of ship plumes and quantification of emissions which was challenging with the predecessor instruments such as GOME (Beirle et al., 2004) and OMI (Boersma et al., 2015). Satellite NO₂ retrieval algorithms have also improved significantly in recent years that allow identifying smaller sources. Georgoulas et al. (2020) for the first time attributed TROPOMI NO₂ plumes from ships in the central Mediterranean to individual ships. Riess et al. (2021) detected several lanes of NO₂ enhancements ranging from the Aegean Sea near Greece to the Skagerrak in Scandinavia, which have not been previously observed with other satellite instruments. Deep learning techniques have been recently introduced to track NO₂ plumes from anthropogenic sources. Finch et al. (2021) uses a convolutional neural network (CNN) to identify the presence of NO₂ plumes using TROPOMI data from different sources. Here we report the development of a deep CNN-based algorithm to detect ship-emitted NO₂ plumes on the ocean at pixel level, improving on the previous work. In other words, our algorithm outlines the mask of each ship-emitted NO₂ plume at pixel-level, going beyond the mere existence of plumes in a TROPOMI data frame. Section 2 introduces the data and method in our study. Section 3 presents results and section 4 concludes our study with discussions and summary.

2. Data and Method

2.1 Data

We use the retrieved NO₂ tropospheric vertical column density (TVCD) from TROPOMI. TROPOMI is a UV-VIS-NIR-SWIR instrument (Veefkind et al., 2012) on board the European Copernicus Sentinel-5 Precursor (S5-P) satellite that was launched on October 13, 2017. It measures solar backscatter radiance and irradiance data with spectral resolutions of approximately 0.5 nm. The ratio of radiance to irradiance at wavelengths between 405 and 465 nm is used to retrieve NO₂ amounts. The ground footprint size is 3.5×5.5 km² (3.5×7 km² before August, 2019) at nadir. It provides nearly daily global coverage with a local equator crossing

time close to 13:30 h. We use the version 1.2.2 TROPOMI Level 2 offline tropospheric NO₂ data products for 2019. TROPOMI NO₂ products have since evolved and improved in newer versions, and there are alternative retrieval schemes available (Lamsal et al., 2022). Our focus here is to demonstrate the applicability our method, which is not sensitive to specific retrievals. We use only observations with quality assurance values > 0.75 to remove cloudy observations.

Training data is built using TROPOMI NO₂ tropospheric retrieval data (Figure 1). We built a graphical user interface program in Python to allow labeling ship-emitted NO₂ within each TROPOMI granule. We compared the NO₂ VCD map with the shipping route map over the Indian ocean. We manually labeled the areas of NO₂ enhancement in the graphical user interface when they are located along the shipping routes. Details on masking procedure and illustrations are presented in Section 3.

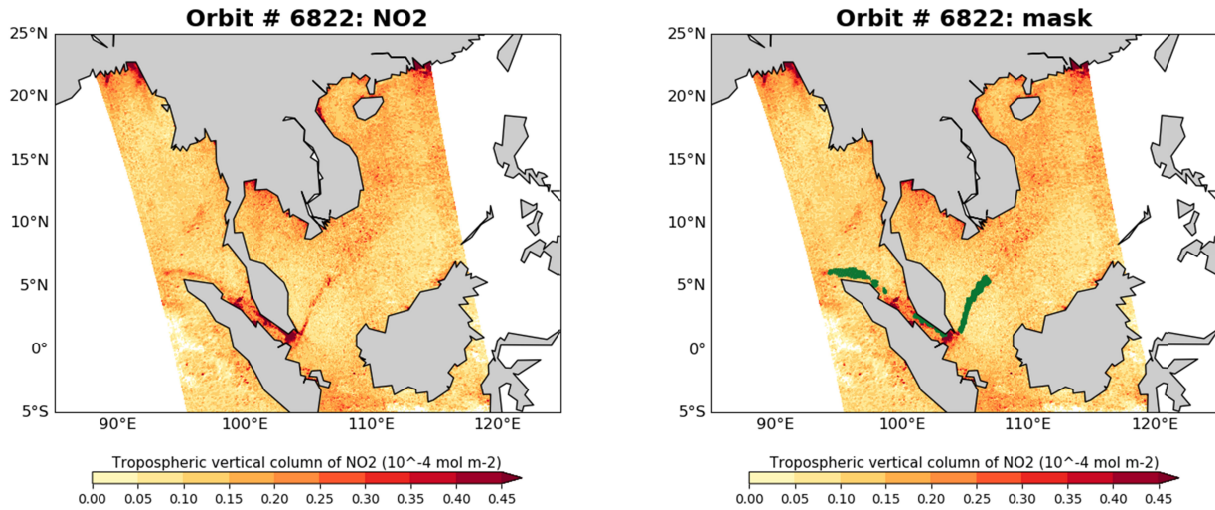


Figure 1: Tropospheric NO₂ retrievals over the Indian ocean. Data are from TROPOMI orbit 6822 on Feb 6th, 2019. There are hot spots along the coastlines that surround the South China Sea and Indian Ocean, the Strait of Malacca, and the Gulf of Thailand. There are also two long ship-emitted plumes emanating from Singapore and coming out of the Strait of Malacca, respectively, as shown in the left panel. The right panel shows the masks reported by our model overlaid on the NO₂ data.

2.2 Using a deep learning model to detect NO₂ plumes

We use an encoder-decoder model to detect ship-emitted NO₂ plumes at the pixel level. As the name suggests, it is made up of an encoder and a decoder, with connections between the two to achieve our goal. Mathematically, the encoder takes input \mathbf{X} , in our case the TROPOMI NO₂ column retrievals, and encoded into higher level features \mathbf{Y} through a multi-layer CNN: $\mathbf{Y} = F_W(\mathbf{X}) + \mathbf{b}$, where F_W represents the neural network model with weight matrix W and biases \mathbf{b} ; then \mathbf{Y} , the features, is decoded back into \mathbf{Z} : $\mathbf{Z} = F'_W(\mathbf{Y}) + \mathbf{b}'$, whose size is the same as \mathbf{X} . The loss function is the distance between \mathbf{Z}^0 and \mathbf{Z} : $\|\mathbf{Z} - \mathbf{Z}^0\|$, where \mathbf{Z}^0 is the pixel-level ground truth plume masks that are created by human experts. We can then train the model to minimize the loss: $W^{l*} = \arg \arg$ and $b^{l*} = \arg \arg$, where W^{l*} and b^{l*} are optimal configurations of the trained model.

Our model architecture is built with a pretrained ResNet-50 as the backbone and adding an additional layer of encoder block (Figure 2). The block consists of three dilated convolutional layers with different dilation rates, 6, 12, and 18, respectively, an image wide pooling layer, and a 1x1 convolutional layer. Their outputs are stacked together and go through a depth-wise convolutional layer. The input data matrix is of size 400x400. It is first resized and goes through a pre-trained ResNet-50 model to get lower-level features, which are fed to the encoder. The low lever features are also fed to the decoder using a 1x1 convolutional layer. The output of the encoder is then upsampled by 4 times through bilinear interpolation. The low-level features and the upsampled encoder features are then concatenated before going through a 3x3 convolutional layer whose output is upsampled again back to 400x400 to make the final prediction.

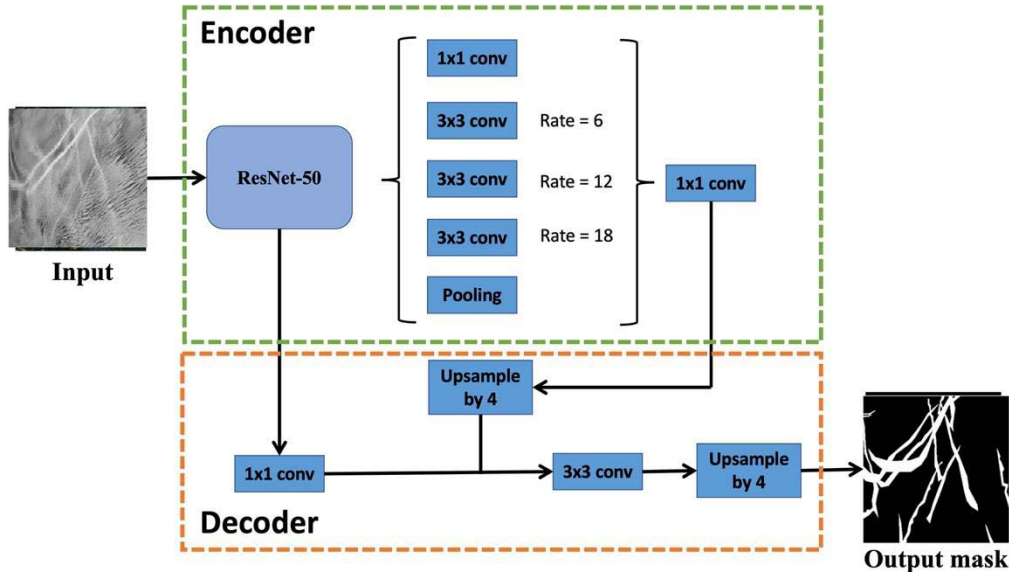


Figure 2: The encoder-decoder architecture employed in our study. Its encoder contains a backbone network, ResNet-50, whose features are fed to the block with three convolutional layers with different rates of dilations, a pooling layer, and 1x1 convolutional layer. Their outputs are concatenated and go through a 1x1 convolutional layer. The decoder accepts features from the ResNet-50 and the output from the encoder.

The model is trained in a supervised fashion with a transfer learning technique. Training and test datasets are prepared with an 80/20 split. Training data contains more than 1000 blocks of size 400x400. The model is not trained from scratch, but with its initial weights set to those from our cloud ship-track detection model (Yuan et al., 2022) because the cloud ship-track and the ship-emitted NO₂ plumes have some common visual features. The model converges faster and easier in this fashion than when the model is trained from scratch. We use a large input size of 400x400 for the model because ship-emitted NO₂ plumes can be hundreds of kilometers long and our model needs a large enough spatial context to detect them. Training data are augmented by rotating and flipping each 400x400 block to increase the robustness of the model.

The model is trained with a A100 graphical processing unit (GPU) with a batch size of 16 using the Adam optimization algorithm (Kingma and Ba, 2014). We use the cross entropy as our loss function.

We train the model until the loss stabilizes after around 40 epochs of training. We measured the model’s performance with the intersection over union (IOU),

$$IOU = \frac{1}{N} \sum_1^N \frac{Y_{pred} \cap Y_{true}}{Y_{pred} \cup Y_{true}},$$

where N is the number of training images. An IOU of 100% means the predicted values match exactly the ‘ground truth’, the human labelled masks in our case. Any mis-match between the prediction and ground truth will result in a decrease in IOU. Our model achieves an IOU of 87% on test data.

3. Results

3.1 Example blocks

In Figure 3, we present a few examples with blocks of NO₂ data, their ground truth labels, and model detected plume masks to illustrate the model performance. The first example shows a negative case, i.e., there is no ship-emitted plumes present. However, there are several NO₂ plumes or hot-spots in the data block. Our model correctly reports no detection of ship-emitted NO₂ plumes in this case. The third example represents a more challenging case where ship-emitted plumes are mixed with many NO₂ plumes and hot-spots that are not ship-emitted in the same data block. Our model correctly detects the true positive plume and ignores the negatives. The second example shows two disjointed short plumes produced by ships around the Strait of Malacca. The trained model manages to detect the plumes correctly. It is worth pointing out that human labels often do not trace out fine-scale variations in the shape of individual plumes because it can be challenging and much more time consuming. The trained model, however, appears to understand the essence of what defines a plume and can trace out fine-scale variations by itself (see examples b, c, and d in Figure 3). This is a sign of good model generalization since it is capturing the true signals. The fourth example shows long ship-emitted plumes mixed with NO₂ hot-spots over both land and ocean. Our model correctly detects true positive plumes and ignores the rest.

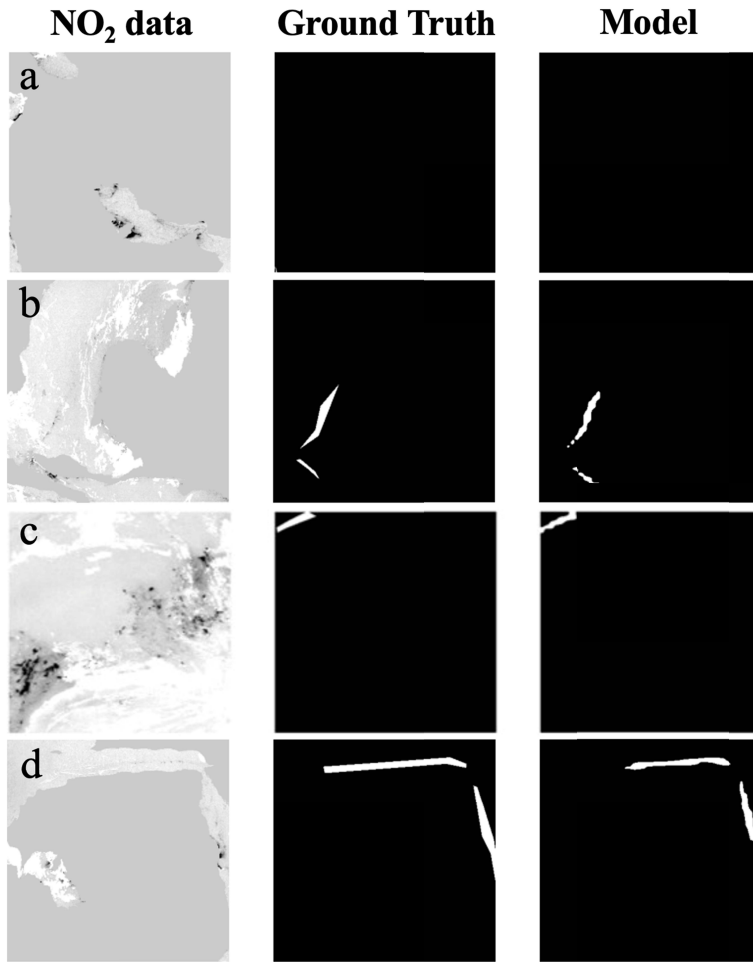


Figure 3: Four example blocks of NO₂ raw data, ground truth labels by human experts, and model predicted plume masks. The model performance is self-evident in these examples. First example shows the presence of multiple NO₂ plumes, but they are not ship-emitted plumes and the model correctly avoids flagging non-ship plumes. In the second example, we show true positives of short plumes. The third shows a mixture of ship-emitted plumes and other hot-spots and the model correctly detects the true positives. The fourth examples shows long ship plumes around the Arabian Peninsula.

3.2 Model performance on a full orbit of TROPOMI data

In Figure 1, we illustrated the performance of our trained model on an orbit of NO₂ data. This orbit is part of our test dataset. We first split the data into 400x400 blocks and apply our model on individual blocks. The masks from individual block predictions are then put back into an orbit of masks with the same dimension as the NO₂ data. We filter out NO₂ data over the land. Two ship-emitted plumes are visible in the raw NO₂ data. They are a few hundred kilometers long. Our model correctly detects both under complex environment. We test the impact of data sampling on the performance of our model. The question we want to address is whether our model can detect a complete plume if it is split in two, or more, 400x400 blocks. Based on multiple case studies, our model correctly detects the same plume if it is split into two blocks.

3.3 Applying the model on one year of TROPOMI

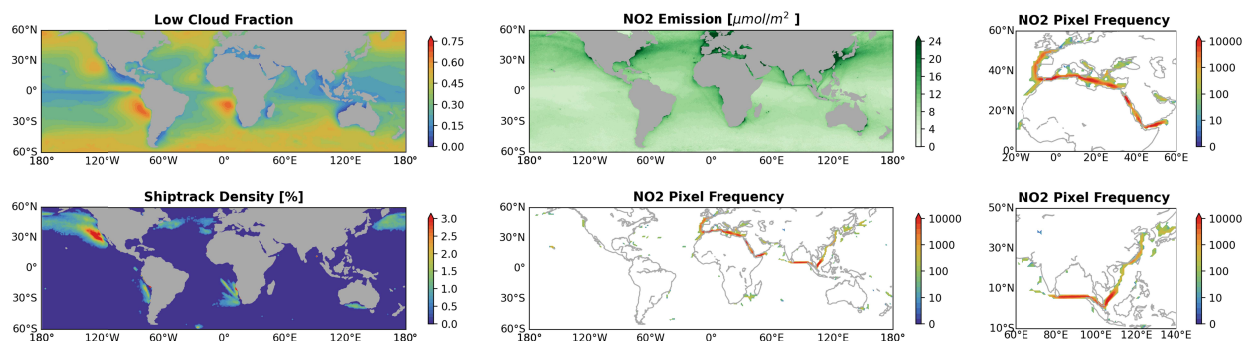


Figure 4: Global distribution of the number of ship-emitted NO₂ plume pixels, low altitude cloud fraction from MODIS, cloud ship-tracks density from our previous work (Yuan et al., 2022), and mean NO₂ concentration using TROPOMI retrievals in 2019 as a proxy for shipping traffic patterns. The distribution pattern clearly follows the shipping lanes. Many parts of the shipping lanes do not show up in this map mainly because of clouds, which prevents TROPOMI from observing tropospheric NO₂ VCD. The right two panels show detected NO₂ plumes frequency for the East Asia and Mediterranean Sea regions.

Here we present results of applying the trained model on global TROPOMI data during 2019. There are more than 5000 orbits of data. The orbital level 2 data are first chopped into 400x400 blocks and we apply our model on them. We then aggregate the number of plume mask pixels that our model detects into 1°x1° grids and plot them with log10 scale in Figure 4. In Figure 4, we also show low cloud fraction climatology from MODIS, cloud ship-tracks distribution (Yuan et al., 2022), and the pattern of NO_x emissions. Figure 4 shows clear patterns of shipping lanes that connect the North Sea near northwestern Europe, the Mediterranean Sea, the Red Sea, the Indian Ocean, through the Strait of Malacca, to the South China Sea and other seas in the east Asia. There are also two minor shipping lanes visible emanating from northern Japan, which may represent shipping traffic between Asia and the Americas. Compared with NO_x emissions and ship-track patterns, the pattern of NO₂ plumes misses shipping lanes in the Southeast Pacific, Northeast Pacific, Southeast Atlantic, Northern Pacific, and Northern Atlantic, and the one to the south of Australia. This can be understood by examining the cloud fraction plot. All these regions have high fraction of low clouds. The low clouds can effectively block any signal from NO₂ plumes. Or, alternatively NO₂ plumes are broken up by cloud fields and rendered not visible from TROPOMI. Indeed, the patterns of cloud ship-tracks that are produced by ship-emitted aerosols interacting with low clouds and NO₂ is complementary to each other. Regions with high ship-track frequencies contain few NO₂ plumes and vice versa. These two would form a more complete global shipping traffic pattern when put together, compared to the NO_x emission map.

The results are encouraging since they indicate that our model generalizes well for each region around the globe and does not produce spurious false positives while capturing the true positives (Figures 1 and 3). The fact that the number of NO₂ mask pixels is strongly regulated by the cloud fraction also makes physical sense, which provides further evidence that our model performs well. We also highlight the distribution of detected plumes for the regions around East Asia and the Mediterranean Sea. The maps show that our algorithm not only captures the main shipping lanes, but also finer shipping routes within each large region such as the shipping activities within the Adriatic Sea, the Black Sea, and the Sea of Japan.

There are a few other less prominent hot spots in the NO₂ density map. For example, there is a minor shipping lane between southern Africa and Madagascar that produces visible but fewer NO₂ plumes, which matches with the low NO_x emissions for the same region. There are some plumes detected along the coast of the Northwest US, near the Aleutian Islands, to the southeast of Australia, and isolated spots in the North Atlantic. These plumes are detected probably when low cloud fraction is low.

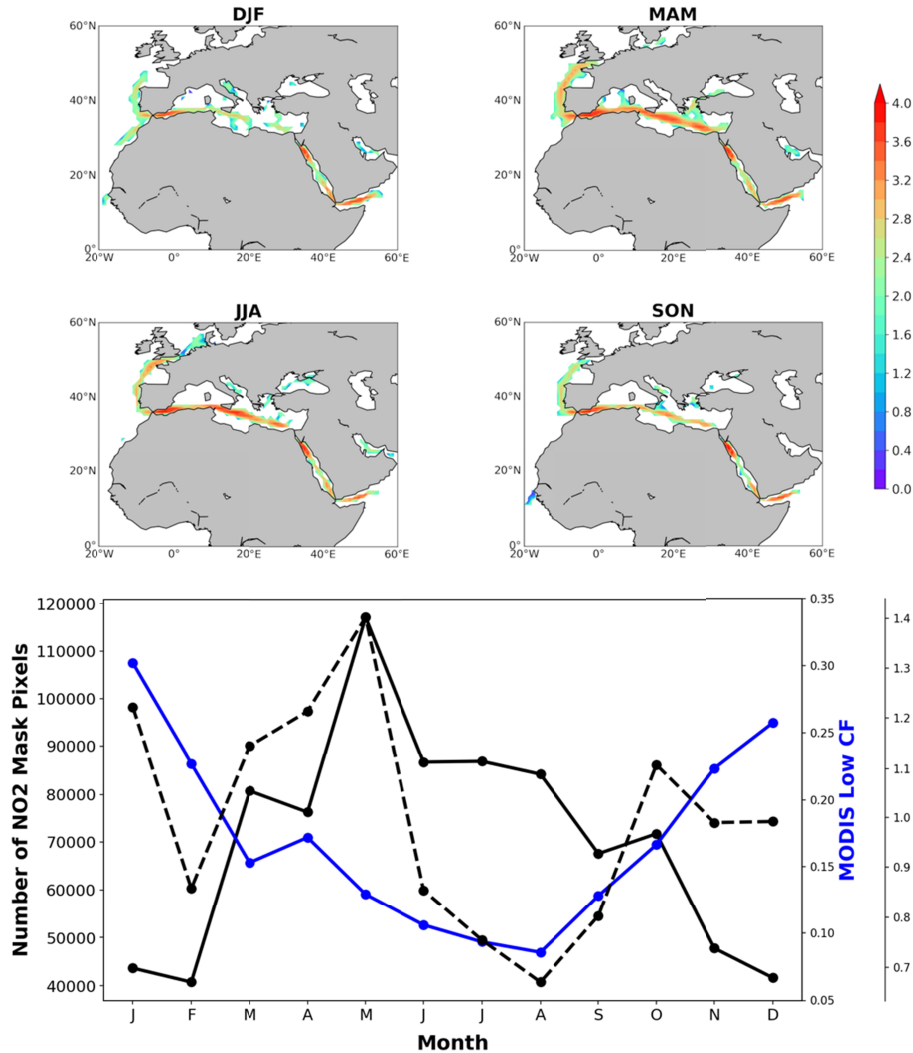


Figure 5: upper panel) Similar to Figure 4, but here the data are separated into different seasons: Dec-Jan-Feb (DJF), Mar-Apr-May (MAM), Jun-Jul-Aug (JJA), and Sep-Oct-Nov (SON). Lower panel) Monthly time series of NO₂ plume pixel counts (black solid line), low cloud fraction (blue line), and normalized pixel counts (black dashed line) over the Mediterranean region between 12°N and 50°N and 8°W and 50°E.

We also examine the seasonal changes of detected NO₂ plumes as shown in Figure 5 where the number of NO₂ plume pixels are mapped for different seasons. There are strong seasonal changes in the number of detected NO₂ plumes around the globe. A few factors can contribute to these seasonal changes such as seasonal variations in shipping traffic, NO_x emissions and lifetime, and cloud conditions. To illustrate the impact of cloud conditions, we focus on the Mediterranean Sea region as shown in Figure 5 lower panel, which shows the time series of the

raw number of detected NO₂ plume pixels, the maritime low cloud fraction, and the pixel number normalized by cloud fraction. It is clear that cloud situation has a strong impact on the detected pixel number as expected. We attempt to remove the effect of cloud fraction on the plume pixel numbers by multiplying the pixel number data by cloud fraction and then dividing the product by its mean. In the normalized data, meaningful variations of around +/- 30% remain, which points to effects from changes in ship traffic and/or atmospheric composition and condition.

4. Discussions and conclusions

In this paper, we focus on detecting ship emitted NO₂ plumes in TROPOMI data. The detection of plumes can be used to improve our estimate of ship NO_x emissions and to verify the compliance and effect of emission control policies (e.g., Yuan et al., 2022). The same method can be extended to detecting NO₂ plumes from tenuous land sources. The method can be enhanced and applied to detect other sources and plumes of not only NO₂ but also of other atmospheric trace gases.

The uncertainty in NO₂ retrievals could hinder the detection of shipping NO₂ plumes. Satellite retrievals of tropospheric NO₂ VCDs consist of three steps (Lamsal et al., 2021): (1) retrievals of NO₂ slant column density (SCD) using the differential optical absorption spectroscopy (DOAS) method, (2) subtracting the stratospheric contribution from the SCD to obtain the tropospheric SCD, and (3) converting the tropospheric SCD to the tropospheric VCD by using the calculated air mass factor (AMF). The subtraction of stratospheric NO₂ components is expected to be a major source of error for the tropospheric VCD in clean background (over sea in this study). TROPOMI NO₂ AMF is based on a-priori NO₂ profiles taken from model simulations at a coarse spatial resolution of 1.0 deg * 1.0 deg, which could cause artificial ship tracks in tropospheric NO₂ data. Additionally, the uncertainties in retrieved cloud pressure and cloud radiance fractions (Lamsal et al., 2021) may add subpixel variabilities for pixels with broken clouds. Improved NO₂ retrievals will help us to detect NO₂ plumes and infer NO_x emissions with higher confidence and reduced uncertainty.

In summary, we developed a deep neural network-based model to detect ship-emitted NO₂ plumes over the ocean. It achieves 87% IOU on independent test data and generalizes well to unseen data. We show it can successfully detect plumes of different sizes and skillfully avoids reporting false positives under complex NO₂ scenes. When applied to one year of TROPOMI data, model detections show major shipping lanes connecting western Europe through Mediterranean Sea, the Arabian Sea, and the Indian Ocean to East Asia, which showcases its performance. Our model does not detect other major shipping lanes because of high cloud cover. Our method can be useful for various applications such as better constraining ship emissions of NO_x, emission compliance verification and policy impact.

Open Research

The TROPOMI NO₂ retrievals are available at <https://scihub.copernicus.eu/>. Search for keywords Sentinel 5 TROPOMI tropospheric NO₂ data once logged in.

Reference

- Aristeidis, K. G., Klaas Folkert, B., Jasper van, V., Xiumei, Z., Ronald van der, A., Prodromos, Z., and Jos de, L.: Detection of NO₂ pollution plumes from individual ships with the TROPOMI/S5P satellite sensor, *Environ. Res. Lett.*, 2020.
- van der A, R. J., de Laat, A. T. J., Ding, J., and Eskes, H. J.: Connecting the dots: NO_x emissions along a West Siberian natural gas pipeline, *npj Clim Atmos Sci*, 3, 1–7, <https://doi.org/10.1038/s41612-020-0119-z>, 2020.
- Beirle, S., Platt, U., von Glasow, R., Wenig, M., and Wagner, T.: Estimate of nitrogen oxide emissions from shipping by satellite remote sensing, *Geophys. Res. Lett.*, 31, L18102, <https://doi.org/doi:10.1029/2004GL020312>, 2004.
- Beirle, S., Boersma, K. F., Platt, U., Lawrence, M. G., and Wagner, T.: Megacity Emissions and Lifetimes of Nitrogen Oxides Probed from Space, *Science*, 333, 1737–1739, <https://doi.org/10.1126/science.1207824>, 2011.
- Beirle, S., Borger, C., Dörner, S., Li, A., Hu, Z., Liu, F., Wang, Y., and Wagner, T.: Pinpointing nitrogen oxide emissions from space, *Science Advances*, 5, eaax9800, <https://doi.org/10.1126/sciadv.aax9800>, 2019.
- Beirle, S., Borger, C., Dörner, S., Eskes, H., Kumar, V., de Laat, A., and Wagner, T.: Catalog of NO_x emissions from point sources as derived from the divergence of the NO₂ flux for TROPOMI, *Earth Syst. Sci. Data*, 13, 2995–3012, <https://doi.org/10.5194/essd-13-2995-2021>, 2021.
- K. Folkert Boersma, Geert, C. M. V., and Jean, T.: Ships going slow in reducing their NO_x emissions: changes in 2005–2012 ship exhaust inferred from satellite measurements over Europe, *Environ. Res. Lett.*, 10, 074007, 2015.
- Capaldo, K., Corbett, J. J., Kasibhatla, P., Fischbeck, P., and Pandis, S. N.: Effects of ship emissions on sulphur cycling and radiative climate forcing over the ocean, *Nature*, 400, 743–746, <https://doi.org/10.1038/23438>, 1999.
- Coakley, J. A., Bernstein, R. L., and Durkee, P. A.: Effect of Ship-Stack Effluents on Cloud Reflectivity, *Science*, 237, 1020–1022, <https://doi.org/10.1126/science.237.4818.1020>, 1987.
- Conover, J. H.: Anomalous cloud lines, *Journal Of The Atmospheric Sciences*, 23, 778–785, [https://doi.org/10.1175/1520-0469\(1966\)023<0778:ACL>2.0.CO;2](https://doi.org/10.1175/1520-0469(1966)023<0778:ACL>2.0.CO;2), 1966.
- Corbett, J. J. and Koehler, H. W.: Updated emissions from ocean shipping, *Journal of Geophysical Research: Atmospheres*, 108, <https://doi.org/10.1029/2003JD003751>, 2003.
- Corbett, J. J., Lack, D. A., Winebrake, J. J., Harder, S., Silberman, J. A., and Gold, M.: Arctic shipping emissions inventories and future scenarios, *Atmospheric Chemistry and Physics*, 10, 9689–9704, <https://doi.org/10.5194/acp-10-9689-2010>, 2010.

Finch, D., Palmer, P., and Zhang, T.: Automated detection of atmospheric NO₂ plumes from satellite data: a tool to help infer anthropogenic combustion emissions, *Atmospheric Meas. Tech. Discuss.*, 1–21, <https://doi.org/10.5194/amt-2021-177>, 2021.

Goldberg, D. L., Lu, Z., Streets, D. G., de Foy, B., Griffin, D., McLinden, C. A., Lamsal, L. N., Krotkov, N. A., and Eskes, H.: Enhanced capabilities of TROPOMI NO₂: Estimating NO_x from North American cities and power plants, *Environ. Sci. Technol.*, 53, 12594–12601, <https://doi.org/10.1021/acs.est.9b04488>, 2019.

International Maritime Organization: IMO 2020 Sulfur Oxide Emission Regulation, 2020.

Kingma, D. P. and Ba, J.: Adam: A Method for Stochastic Optimization, arXiv:1412.6980 [cs], 2014.

Lamsal, L. N., Krotkov, N. A., Vasilkov, A., Marchenko, S., Qin, W., Yang, E.-S., Fasnacht, Z., Joiner, J., Choi, S., Haffner, D., Swartz, W. H., Fisher, B., and Bucsela, E.: Ozone Monitoring Instrument (OMI) Aura nitrogen dioxide standard product version 4.0 with improved surface and cloud treatments, *Atmospheric Measurement Techniques*, 14, 455–479, <https://doi.org/10.5194/amt-14-455-2021>, 2021.

Lamsal, L.N., Nickolay A. Krotkov, Sergey V. Marchenko, Joanna Joiner, Luke Oman, Alexander Vasilkov, Bradford Fisher, Wenhan Qin, Eun-Su Yang, Zachary Fasnacht, Sungyeon Choi, Peter Leonard, and David Haffner (2022), TROPOMI/S5P NO₂ Tropospheric, Stratospheric and Total Columns MINDS 1-Orbit L2 Swath 5.5 km x 3.5 km, NASA Goddard Space Flight Center, Goddard Earth Sciences Data and Information Services Center (GES DISC), [10.5067/MEASURES/MINDS/DATA203](https://disc.gsfc.nasa.gov/datasets/TROPOMI_S5P_NO2_TSC_MINDS_1-Orbit_L2_Swath_5.5km_x_3.5km/versions/1)

Laughner, J. L. and Cohen, R. C.: Direct observation of changing NO_x lifetime in North American cities, *Science*, 366, 723–727, <https://doi.org/10.1126/science.aax6832>, 2019.

Liu, F., Beirle, S., Zhang, Q., Dörner, S., He, K., and Wagner, T.: NO_x lifetimes and emissions of cities and power plants in polluted background estimated by satellite observations, *Atmospheric Chem. Phys.*, 16, 5283–5298, <https://doi.org/10.5194/acp-16-5283-2016>, 2016.

Liu, F., Page, A., Strode, S. A., Yoshida, Y., Choi, S., Zheng, B., Lamsal, L. N., Li, C., Krotkov, N. A., Eskes, H., van der A, R., Veefkind, P., Levelt, P. F., Hauser, O. P., and Joiner, J.: Abrupt decline in tropospheric nitrogen dioxide over China after the outbreak of COVID-19, *Science Advances*, 6, eabc2992, <https://doi.org/10.1126/sciadv.abc2992>, 2020.

Lorente, A., Boersma, K. F., Eskes, H. J., Veefkind, J. P., van Geffen, J. H. G. M., de Zeeuw, M. B., Denier van der Gon, H. A. C., Beirle, S., and Krol, M. C.: Quantification of nitrogen oxides emissions from build-up of pollution over Paris with TROPOMI, *Sci. Rep.*, 9, 20033, <https://doi.org/10.1038/s41598-019-56428-5>, 2019.

Miyazaki, K., Eskes, H., Sudo, K., Boersma, K. F., Bowman, K., and Kanaya, Y.: Decadal changes in global surface NO_x emissions from multi-constituent satellite data assimilation,

- Atmospheric Chemistry and Physics, 17, 807–837, <https://doi.org/10.5194/acp-17-807-2017>, 2017.
- Richter, A., Eyring, V., Burrows, J. P., Bovensmann, H., Lauer, A., Sierk, B., and Crutzen, P. J.: Satellite measurements of NO₂ from international shipping emissions, *Geophys. Res. Lett.*, 31, L23110, <https://doi.org/10.1029/2004GL020822>, 2004.
- Richter, A., Burrows, J. P., Nüß, H., Granier, C., and Niemeier, U.: Increase in tropospheric nitrogen dioxide over China observed from space, *Nature*, 437, 129–132, <https://doi.org/10.1038/nature04092>, 2005.
- Riess, T. C. V. W., Boersma, K. F., van Vliet, J., Peters, W., Sneep, M., Eskes, H., and van Geffen, J.: Improved monitoring of shipping NO₂ with TROPOMI: decreasing NO_x emissions in European seas during the COVID-19 pandemic, *Atmospheric Meas. Tech. Discuss.*, 1–35, <https://doi.org/10.5194/amt-2021-321>, 2021.
- Veefkind, J. P., Aben, I., McMullan, K., Förster, H., de Vries, J., Otter, G., Claas, J., Eskes, H. J., de Haan, J. F., Kleipool, Q., van Weele, M., Hasekamp, O., Hoogeveen, R., Landgraf, J., Snel, R., Tol, P., Ingmann, P., Voors, R., Kruizinga, B., Vink, R., Visser, H., and Levelt, P. F.: TROPOMI on the ESA Sentinel-5 Precursor: A GMES mission for global observations of the atmospheric composition for climate, air quality and ozone layer applications, *Remote Sens. Environ.*, 120, 70–83, 2012.
- Vinken, G. C. M., Boersma, K. F., van Donkelaar, A., and Zhang, L.: Constraints on ship NO_x emissions in Europe using GEOS-Chem and OMI satellite NO₂ observations, *Atmospheric Chemistry and Physics*, 14, 1353–1369, <https://doi.org/10.5194/acp-14-1353-2014>, 2014.
- Yuan, T., Remer, L. A., and Yu, H.: Microphysical, macrophysical and radiative signatures of volcanic aerosols in trade wind cumulus observed by the A-Train, *Atmospheric Chemistry And Physics*, 11, 7119–7132, <https://doi.org/10.5194/acp-11-7119-2011>, 2011.
- Yuan, T., Song, H., Wang, C., Oreopoulos, L., Platnick, S. E., von Hippel, S., Meyer, K. G., Light, S., and Wilcox, E.: Global Reduction in Ship-tracks from Sulfur Regulations for Shipping Fuel, *Science Advances*, Vol 8, Issue 29, [DOI: 10.1126/sciadv.abn7988](https://doi.org/10.1126/sciadv.abn7988), 2022.